STRUCTURAL BIOLOGY COMMUNICATIONS

ISSN 2053-230X

Protein crystallization and initial neutron diffraction studies of the photosystem II subunit PsbO

Martin Bommer,[a]*‡§ Leighton Coates,[b]*¶ Holger Dau,[c] Athina Zouni[a] and Holger Dobbek[a]

[a]Institut für Biologie, Humboldt-Universität zu Berlin, Unter den Linden 6, 10099 Berlin, Germany, [b]Biology and Soft Matter Division, Oak Ridge National Laboratory, 1 Bethel Valley Road, Oak Ridge, TN 37831, USA, and [c]Fachbereich Physik, Freie Universität Berlin, Arnimallee 14, 14195 Berlin, Germany. *Correspondence e-mail: martin.bommer@gmx.net, coatesl@ornl.gov

Received 26 June 2017
Accepted 22 August 2017

Edited by G. G. Privé, University of Toronto, Canada

‡ Questions about the crystallization experiment should be addressed to MB.
§ Present address: Max-Delbrück-Centrum, Robert-Rössle-Strasse 10, 13125 Berlin, Germany.
¶ Questions about the neutron diffraction experiment should be addressed to LC.

Keywords: photosystem II; PsbO; counter-diffusion; agarose; neutron diffraction; capillary; cross-linking.

Supporting information: this article has supporting information at journals.iucr.org/f

The PsbO protein of photosystem II stabilizes the active-site manganese cluster and is thought to act as a proton antenna. To enable neutron diffraction studies, crystals of the β-barrel core of PsbO were grown in capillaries. The crystals were optimized by screening additives in a counter-diffusion setup in which the protein and reservoir solutions were separated by a 1% agarose plug. Crystals were cross-linked with glutaraldehyde. Initial neutron diffraction data were collected from a 0.25 mm^3 crystal at room temperature using the MaNDi single-crystal diffractometer at the Spallation Neutron Source, Oak Ridge National Laboratory.

1. Introduction

Photosystem II (PSII) is one of the key enzymes in oxygenic photosynthesis, which is responsible for aerobic life on Earth. This ensures the release of oxygen into the atmosphere, which keeps us alive while also providing us with food. Oxygen release in PSII takes place at a catalytic hetero-metal cluster Mn_4CaO_5, whereby water is oxidized and additional protons and electrons are released. The PSII core complex from cyanobacteria is a dimer, in which each monomer consists of 20 different protein subunits. 17 are membrane-intrinsic (D1/D2, CP47/CP43, Cyt b_{559}, PsbH–PsbM, PsbT, PsbX, PsbY, PsbZ and Ycf12) and three are membrane-extrinsic and bound to the luminal side (PsbO, PsbU and PsbV) (Hellmich *et al.*, 2014; Umena *et al.*, 2011). The β-barrel core of PsbO protrudes prominently from the structures of cyanobacterial (Ferreira *et al.*, 2004; Umena *et al.*, 2011; Zouni *et al.*, 2001), red algal (Ago *et al.*, 2016) and plant (Wei *et al.*, 2016) PSII, while three loops (residues 55–63, 149–192 and 220–231 in *Thermosynechococcus elongatus* PsbO) tightly interact with the central PSII subunits CP47/43 and D2. The loops are thought to be unstructured in isolated PsbO in solution, and NMR experiments have confirmed large unstructured regions (Nowaczyk *et al.*, 2004). While the basic PsbO structure is evolutionarily conserved, significant species-dependent variations exist in the surface-exposed amino acids and connecting loops. The variations in the number and the location of charged residues, which are likely to be functionally relevant, have recently been analyzed for more than 70 nonredundant sequences from cyanobacteria and plants (Del Val & Bondar, 2017).

It can be concluded that the PsbO protein seems to have key functions in all oxygenic organisms. The following

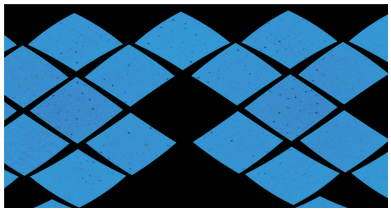

functions of the PsbO subunit in the PSII core complex have already been discussed in the literature: (i) it stabilizes the protein-bound water-splitting Mn_4Ca-oxo cluster and (ii) it is assumed to conduct protons away from the cluster site into the bulk solvent (Bondar & Dau, 2012; De Las Rivas & Barber, 2004; Ifuku, 2015; Popelkova & Yocum, 2011; Roose *et al.*, 2016; Shutova *et al.*, 2007).

More than 20 carboxylate side chains are present on the surface of PsbO, which are often not isolated but are arranged in the form of carboxylate clusters (Bommer *et al.*, 2016). These carboxylate clusters have been proposed to serve as 'proton antennae' (Bondar & Dau, 2012; Shutova *et al.*, 2007). The term proton antenna was coined to discuss the putative functional role of surface-exposed protonatable side chains (of Asp, Glu and His; Ädelroth & Brzezinski, 2004). In PSII-bound PsbO, the proton-antenna functionality may comprise a variety of functions: (i) proton storage (to reduce acidification of the lumenal compartment), (ii) proton conduction along the protein surface of PsbO (to sites that are favourable for proton release) and (iii) accelerated proton transfer to water molecules of the lumenal bulk and/or (iv) neighbouring protein subunits in the lumenal space of the thylakoids, which is densely packed with protein chains of PSII. Although it is commonly assumed that proton antenna play an important role in many redox proteins, the physical chemical basis of the hypothesized functionality of proton antenna is generally ill-understood. One decisive knowledge gap is the unknown protonation state of the carboxylate clusters on the protein surface, which are hydrogen-bonded to a partially structured/partially fluctuating shell of water molecules (Bommer *et al.*, 2016; Lorch *et al.*, 2015). Insight into the structure of the hydrogen-bond networks on the protein surface, including the protonation states of individual carboxylate O atoms and the orientation of nearby water molecules, would represent a crucial step forwards in the endeavour to understand the proton-antenna functionality in biological redox chemistry. Although it is an especially demanding experimental approach, we consider neutron crystallography to be the method of choice to gain the structural information that is needed (O'Dell *et al.*, 2016; Tomanicek *et al.*, 2013; Wan *et al.*, 2015).

In order to study isolated PsbO by high-resolution X-ray and neutron crystallography, we have previously designed a stable core construct containing only the β-barrel of PsbO, named PsbO-β. Loops originating from antiparallel β-strands were replaced with intrinsically stable Asn-Gly β-hairpins (Sibanda *et al.*, 1989; Simpson *et al.*, 2005). PsbO-β thus contains the complete β-barrel with 175 of the original 246 amino-acid residues of full-length PsbO. It is a model system that is highly stable to variations in pH (2–10) and temperature (75°C at pH 6.5).

To analyze this network, we have previously reported X-ray structures of PsbO-β at 100 K and at room temperature (297 K), in which we identified water–carboxylate clusters that are predicted to serve as proton conduits (Bondar & Dau, 2012; Lorch *et al.*, 2015; Shutova *et al.*, 2007) and also discovered a putative pH-controlled structural switch involving the deprotonation of a carboxylate dyad (Bommer *et al.*, 2016). However, as protons were invisible in the electron density, more direct ways to reveal the protonation states of individual amino acids in PsbO are mandatory to obtain further insights into the proton antennae. Here, we show how the previous crystallization conditions can be modified to yield large crystals suitable for neutron diffraction studies, from which a first data set was recorded.

Table 1
Macromolecule-production information.

Source organism	*T. elongatus* BP1
DNA source	Synthetic, assembled DNA
Expression vector	pET-28a (Millipore, Billerica, Massachusetts, USA)
Expression host	*E. coli* BL21(DE3) (Millipore)
Growth conditions	Terrific Broth (TB), 42°C for 5 h post-induction
UniProt entry	p0a431 (modified)
Expression tag	N-terminal *E. coli* thioredoxin (TrxA), hexahistidine, TEV protease site
Amino-acid sequence of tag (removed for crystallization)	MSDKIIHLTDDSFDTDVLKADGAILVDFWAEWCG PCKMIAPILDEIADEYQGKLTVAKLNIDQNPG TAPKYGIRGIPTLLLFKNGEVAATKVGALSKG QLKEFLDANLAGSGSSHHHHHHGSPTTENLYF Q
Crystallized amino-acid sequence†	GHMGTANKCPTLDDTARGAYPIDSSQTYRIARLC LQPTTFLVKENGEFVPTKLVTRETTSLDQIQG ELKVNSDGSLTFVEEDGIDFQPVTVQMAGGER IPLLFTVKNLVASTQPNVTSITTSTDFKGEFN VNGTKGQISLNVAKVDGRTGEIAGTFESEQLS NGHEVKIQGVFYASIEPA

† The underlined residues in PsbO-β replace the deleted loops in wild-type PsbO.

2. Materials and methods

2.1. Macromolecule production

Cloning, expression and purification of PsbO-β have been described previously (Bommer *et al.*, 2016). Crucially, the *Escherichia coli* cells were grown at 42°C in order to enhance soluble expression of the thermophilic protein (Koma *et al.*, 2006). Table 1 lists sequence and other expression parameters, while purification will be described briefly here. The cells were lysed in 30 m*M* MES–NaOH pH 6.5, 200 m*M* NaCl, 1 m*M* PMSF and approximately 0.03 mg ml^{-1} DNAseI. Trx/hexahistidine-tagged PsbO-β was partially purified on Ni-Sepharose HP resin (GE Healthcare Life Sciences, Chicago, Illinois, USA) using 40 m*M* imidazole in the wash buffer and 300 m*M* in the elution buffer. The tag was then cleaved with 1 mg TEV protease per 30 mg PsbO-β for at least 12 h at 4°C, while both proteins were dialysed against 30 m*M* Na MES pH 6.5, 0.5 m*M* EDTA, 1 m*M* DTT. The tag and TEV protease were removed by affinity chromatography using the same Ni-Sepharose HP column. PsbO-β was further purified by gel filtration on Superdex 75 resin (GE Healthcare) in 30 m*M* Na MES pH 6.5, 150 m*M* NaCl and was stored in 30 m*M* Na MES pH 6.0 at −80°C. Purification was routinely carried out at 12°C.

2.2. Crystallization

Screening plates were set up for sitting-drop experiments in MRC plates (Swissci, Neuheim, Switzerland) using the buffers listed in Table 2. Counter-diffusion experiments were also set

up using 1–1.5 mm internal diameter glass capillaries and the buffers and protein solution detailed in Table 2. The agarose 'plug' was prepared as a 1 ml scale solution in a micro-centrifuge tube placed in a heat block set to 85°C. Gel-loading tips were prewarmed on the heat block and used to place 5–10 µl of the agarose into the centre of the glass capillary. Alternatively, a 50 µl Hamilton syringe prewarmed in a beaker of hot water was used. After the plug had hardened, 20–40 µl of the protein solution and twice the volume of precipitant were added flush to either side of the agarose plug and the ends of the capillary tube were then sealed with plasticine or Parafilm.

For in-gel crystallization setups, the plug and precipitate were prepared as above. In addition to the agarose plug, the protein side of the capillary was turned into a gelled liquid. A fourfold stock solution was prepared from 1.6% low-melting-point agarose in water. Taking advantage of the thermophilic origin of PsbO-β, the protein and agarose solutions were both

Table 2
Crystallization.

Method	Vapour diffusion	Counter-diffusion
Plate type	MRC Maxi, sitting drop	0.5–2 mm quartz glass capillaries
Temperature (K)	291	291
Protein concentration (mg ml^{-1})	40	80
Buffer composition of protein solution	20 m*M* MES–NaOH pH 6	50 m*M* MES–NaOH pH 6, 5 m*M* calcium acetate, 1 m*M* TCEP
Composition of reservoir solution	100 m*M* MES–NaOH pH 6, 200 m*M* calcium acetate, 10 m*M* TCEP, 30% PEG 400	100 m*M* MES–NaOH pH 6, 20 m*M* calcium acetate, 10 m*M* TCEP, 50% PEG 400
Composition of agarose plug	N/A	1.5% agarose, 50 m*M* MES–NaOH pH 6, 5 m*M* calcium acetate
Volume and ratio of drop	2 + 2 µl	40–80 µl precipitant + 5–10 µl plug + 20–40 µl protein
Volume of reservoir (µl)	100	N/A

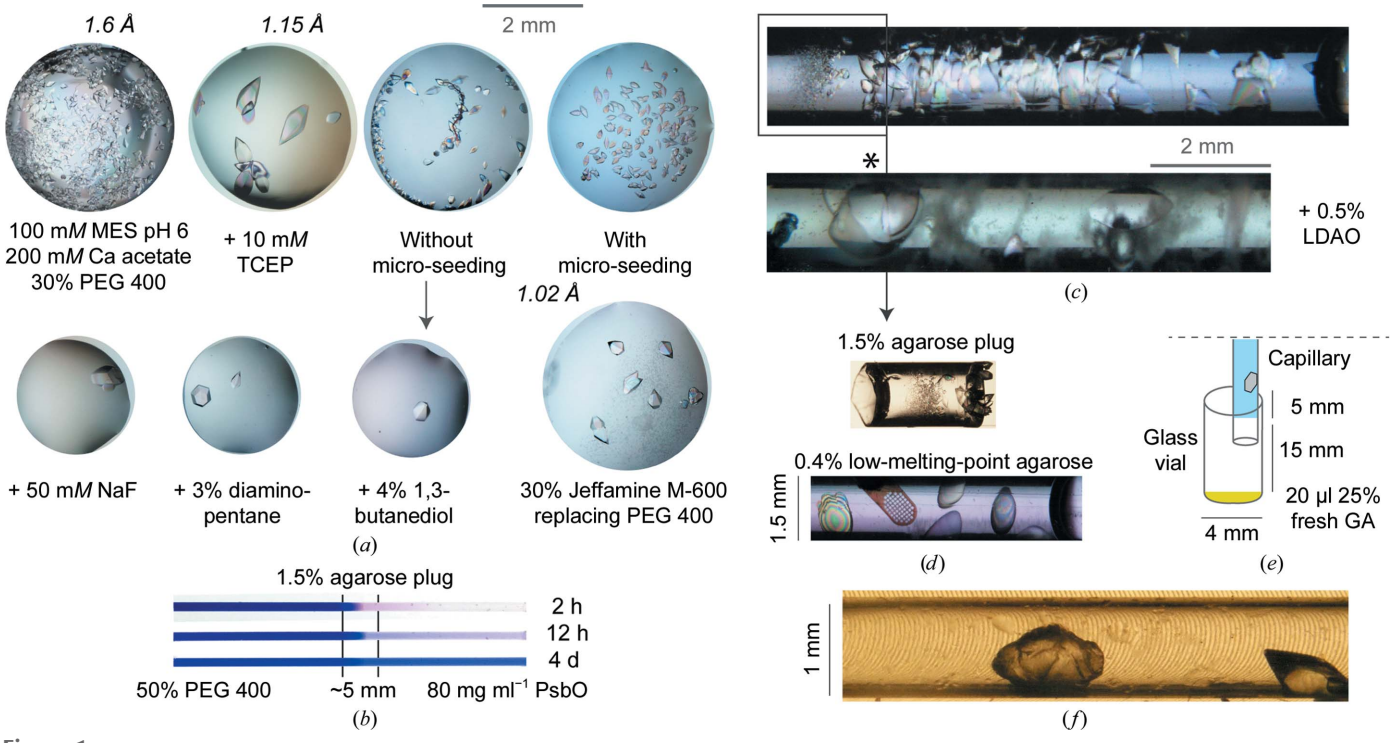

Figure 1
(*a*) Optimization of PsbO-β crystals in MRC2/MRC Maxi sitting-drop plates. All setups contain the initial reservoir solution; all but the initial drop contain 10 m*M* TCEP. Micro-seeding was performed with a 10 000-fold (final) dilution of a crystal broken by vortexing in the presence of a 2 mm glass bead in reservoir buffer for 1 min. Diffraction was tested on beamline 14.1 at BESSY II, HZB (Mueller *et al.*, 2015) and beamline P11 at PETRA III, DESY (Burkhardt *et al.*, 2016) at 100 K from crystals cryocooled straight from the drop. (*b*) Test of the counter-diffusion experiment set up in 1–1.5 mm capillaries. Bromophenol blue (670 Da) was added to the 50% PEG side as a reporter. After 4 d, 25% of it had migrated to the protein side occupied by 80 mg ml^{-1} PsbO-β in (*c*). (*c*) Protein side of two capillaries with 100 m*M* MES pH 6, 200 m*M* calcium acetate, 10 m*M* TCEP, 50% PEG 400 as precipitant. The box locates the agarose plug. The lower capillary shows the crystal used for data collection (indicated with an asterisk). (*d*) The agar plug was removed from the capillary together with the embedded crystals. Below is a capillary setup with low-melting-point agarose included in the protein buffer. (*e*) Schematic of the cross-linking setup for crystal capillaries. 20 µl freshly thawed glutaraldehyde (GA) was placed in a HPLC-vial insert and the open-ended capillary was suspended above. The gap was sealed with Parafilm. (*f*) A cross-linked PsbO-β crystal is shown on the left side of the figure. This H/D-exchanged crystal was used for data collection. The volume of this crystal was approximately 0.25 mm^3.

equilibrated at 45°C, combined and added flush against the agarose plug. [Note that with some care, the agarose solution may be cooled to as low as 35°C and added to the protein solution at room temperature (Sauter *et al.*, 2009).]

2.3. Data collection and processing

Crystals were initially tested at 100 K by X-ray diffraction after cryocooling straight from the drop. Test data sets were collected on beamline 14.1 at BESSY II, HZB, Berlin, Germany (Mueller *et al.*, 2015).

Time-of-flight (TOF) neutron diffraction data from a 0.25 mm^3 PsbO crystal (Fig. 1*f*) at 293 K were initially recorded to 2.30 Å resolution using the Macromolecular Neutron Diffractometer (MaNDi; Coates *et al.*, 2010, 2015) at the Spallation Neutron Source (SNS) at Oak Ridge National Laboratory (ORNL). Data were collected using all neutrons between 2 and 4 Å to give a time-of-flight wavelength-resolved Laue pattern (Coates *et al.*, 2015). Eight images were collected in total with a 10° φ rotation between images, with the crystal being static during the collection of each image. These eight images (Fig. 2) were processed and integrated using the *Mantid* software package (Arnold *et al.*, 2014), with the *LAUENORM* program from the *LAUEGEN* package (Campbell *et al.*, 1998) being used for wavelength normalization of the Laue data and scaling between Laue diffraction images.

3. Results and discussion

We have previously crystallized PsbO-β by sitting-drop or hanging-drop vapour diffusion. The crystallization buffer consisted of 0.2 *M* Na MES pH 6, 25% PEG 400, 0.2 *M* calcium acetate, 10 m*M* tris-(2-carboxyethyl)phosphine hydrochloride (TCEP) (Bommer *et al.*, 2016). TCEP was required to increase the crystal size and improve the X-ray diffraction from 1.6 to 1.2 Å resolution, possibly by avoiding the formation of nonspecific intermolecular cross-links between Cys19 and Cys44 of PsbO-β. However, an intramolecular disulfide bridge between these residues exists *in vivo* (Umena *et al.*, 2011) and is required for correct folding of PsbO when expressed recombinantly in *E. coli* (Nikitina *et al.*, 2008). In the crystal structure of PsbO-β, the inclusion of TCEP leads to partial cleavage of the disulfide bond and associated weakening of the electron density at the stapled N-terminal loop. Calcium binds to a divalent cation-binding site including residues Thr138, Asp141, Asn200 and Val201, which is occupied by calcium in most structures of intact PSII. In crystals of PsbO-β, calcium additionally mediates crystal contacts.

Such crystals grew to 0.2–0.4 mm in the longest dimension by vapour diffusion but did not exceed this size even when the drop volume was increased. We thus considered precipitant buffer optimization, seeding and also counter-diffusion (see below) as possible routes to increase the crystal volume. In a search for buffer components that may lead to fewer, larger, single crystals, the Additive and Detergent Screens (Hampton Research, Aliso Viejo, California, USA) were tested in sitting-drop plates. The largest crystals were obtained with sodium fluoride, diaminopentane and *N*,*N*-dimethyldodecylamine *N*-oxide (LDAO), although fluoride formed a precipitate with calcium and primary amines such as diaminopentane scavenge the glutaraldehyde cross-linking reagent (described below).

Similar results were obtained with other amines [proline, aminohexanoic acid, taurine, sarcosine, spermine, benzylamine, Jeffamine M-600 and nondetergent sulfobetaine (NDSB 201)] and polyalcohols (*myo*-inositol, ethylene glycol, 1,6-hexanediol 1,3-butanediol and propylene glycol). Alternatively, Jeffamine M-600 was able to substitute for PEG 400 as precipitant, leading to larger, well diffracting crystals after a longer time of incubation. However, no crystals were obtained in initial capillary tests as are described below for PEG.

Macro-seeding (Bergfors, 2003) has frequently been used to overcome the limit of the total protein quantity in the drop and the unpredictability of nucleation. Initial attempts to transfer PsbO-β crystals to a fresh drop led to the growth of satellite crystals from damaged points on the crystal but not to an increase in the size of the original crystal. By contrast, drops to which 1000-fold to 10 000-fold diluted seed stock from fragmented crystals had been added produced crystals that were uniform in number and size. A limited optimization experiment, in which the effect of such micro-seeding (Gavira *et al.*, 2011; Shaw Stewart *et al.*, 2011) was tested with varying PEG concentration is shown in Supplementary Fig. S1. However, the largest crystals grew at low (25%) PEG concentrations from the side of the drop in the absence of added seed stock. Lowering the PEG concentration (20%) led to fewer but also smaller crystals.

This experiment sampled only a part of the crystallization optimization space, effectively a line through the phase diagram at an arbitrary protein concentration of 40 mg ml^{-1}. Determination of solubility curves in two-dimensional phase diagrams (frequently protein *versus* precipitant concentration) has previously allowed the design of crystallization experiments yielding large crystals (Ng *et al.*, 2015). Both direct protein solubility measurement (Sauter *et al.*, 1999) and crystal dissolution tests (Nakamura *et al.*, 2013) have been used to estimate solubility curves and thus guide the design of

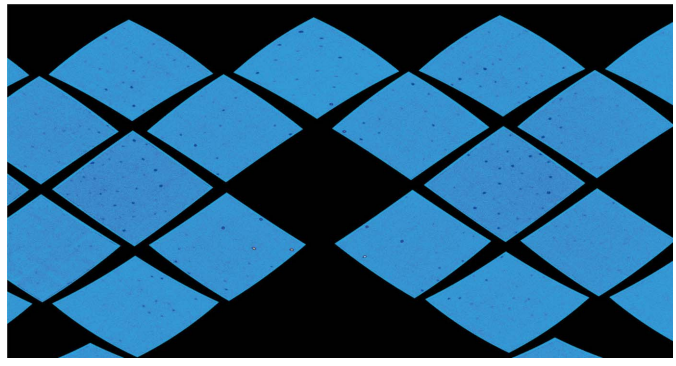

Figure 2
Neutron diffraction peaks from an H/D-exchanged crystal of PsbO-β. For clarity, a selected time-of-flight range across 15 of the 40 MaNDi detector modules is shown.

optimal high protein concentration experiments (Chayen, 2005). However, the rapid gains made by the application of the capillary counter-diffusion method to PsbO-β led us to not fully evaluate optimization of the vapour-diffusion experiment.

Capillary counter-diffusion experiments are common in the production of large crystals for neutron diffraction (Ng *et al.*, 2015). Each capillary samples a wide region of the phase diagram and it may significantly slow the rate of mixing between protein and precipitant. They therefore allow high initial concentrations of protein to be used. To estimate the rate of mixing in glass tubes of sufficient diameter to grow large-size crystals (1–2 mm), we used the dye bromophenol blue as a visual guide (Fig. 1*b*). When protein and precipitant solutions were simply added to either side, the precipitant mixed with the protein within minutes. The corresponding crystallization trials resulted in a uniform distribution of small crystals. In order to slow convection and move the crystallization to a diffusion regime, an ∼5 mm agar plug (Ng *et al.*, 2015) was introduced between the protein and precipitant sides of the capillary. The dye showed that the rate of equilibration slowed to 25% over 4 d, roughly the same time as was taken for the full equilibration of a vapour-diffusion experiment with 4 µl initial drop size. PsbO-β crystals grew within 4–8 d to 1–2 mm in the longest dimension. Additives (amines and polyalcohols) which led to fewer, larger PsbO-β crystals in vapour-diffusion experiments showed the same effect in capillaries. The counter-diffusion setup thus routinely yielded crystals of sufficient size for neutron diffraction.

Crystals frequently grew from the centre of the agarose plug outwards, with several large crystals originating at the interface of the plug and protein chamber. Such crystals diffracted to high resolution but were not easily separated from the solid agarose plug. Agarose solutions at concentrations as low as 0.12% behave like viscoelastic gels, which retain the ability to resist mixing by convection (García-Ruiz *et al.*, 2001) during crystallization and crystal manipulation (Sauter *et al.*, 2009), yet they may be more easily manipulated than solid agar gels. We added 0.4% low-melting-point agarose (a gelled liquid) to the protein side of the capillary in an adaptation of the method of Biertümpfel *et al.* (2002). In the gelled liquid, the crystals grew to the diameter of the capillary in the longest dimension, albeit losing their sharp edges. The X-ray diffraction was comparable to that of other crystals (see Supplementary Fig. S2). As such, the method presented no immediate benefit for the PsbO-β system. However, it may be preferable where the slow diffusion of buffer components or hydrogen–deuterium exchange of sensitive crystals is desired. Manual crystal handling (pipetting or moving the crystal with a nylon loop) was not impaired but osmotic stress from convection of buffer components has been shown to be reduced (García-Ruiz *et al.*, 2001).

Neutron crystallography experiments rely on the replacement of H atoms with the isotope deuterium for detection and refinement (Afonine *et al.*, 2010) of hydrogen positions and for reduction of background scattering (Blakeley, 2009; O'Dell *et al.*, 2016; Oksanen *et al.*, 2017). Crystals of PsbO-β contain 45% solvent, which includes the precipitant. Exchangeable protons bound to polar atoms such as O and N atoms (typically 15–25% in proteins; Kita & Morimoto, 2016; Oksanen *et al.*, 2017) and protein-bound solvent molecules may be replaced by deuterium. These were the focus of our research interest in PsbO. Any remaining H atoms in the sample contribute disproportionately to background scattering (40-fold over deuterium; Blakeley, 2009; Oksanen *et al.*, 2017).

We thus examined the components of our crystal system to help to maximize the exchange of hydrogen to deuterium in PsbO-β and to reduce the percentage of remaining solvent H atoms inside the crystal. Crystallization in D_2O-containing buffers and even refolding of PsbO-β in D_2O/d_4-urea (for a recent example, see Kita & Morimoto, 2016) was successful in the initial experiments, but such a crystal system has not been sufficiently optimized for PsbO-β. Instead, in initial crystallization trials for neutron diffraction our efforts focused on D_2O solvent exchange in H_2O-grown crystals. H_2O was replaced by D_2O and buffer salts were washed in D_2O. The detergent LDAO was identified as an aid to the formation of large crystals. While in membrane-protein crystals detergent hemimicelles are a significant reservoir of H atoms, we do not expect such detergent micelles to be present in the narrow solvent channels of PsbO-β crystals. The precipitant polyethylene glycol contains several non-exchangeable H atoms and we thus attempted to exchange PEG 400 with the commercially available d_6-ethylene glycol.

We were initially successful in transferring several-month-old test crystals to a buffer containing D_2O and 50% d_6-ethylene glycol in place of 30% PEG 400. However, fresh crystals shattered under the same conditions, presumably from the osmotic stress introduced by the desiccant ethylene glycol (Wheeler *et al.*, 2012). We speculated that protein cross-linking might have occurred at the crystal surface of older crystals and that this may protect the crystals from the osmotic shock of moving between different solutions. Such protection from osmotic shock appeared to be useful when transferring the large crystals from an unknown PEG concentration, such as in the part-equilibrated capillary (Fig. 1*b*), to a harvesting solution containing 25% PEG 400 or ethylene glycol. This in turn may allow accelerated deuterium exchange should the crystals of PsbO-β be sufficiently stabilized by cross-linking. Such an approach would represent a short cut tailored to our crystal system. We do note that well established, gentle yet slower procedures exist for such large crystals: crystals may be grown in deuterated buffers. Alternatively, H_2O may be exchanged for D_2O after crystallization by vapour diffusion in the capillary (Ng *et al.*, 2015). The approach requires no crystal handling and reduces osmotic shock. It is more suited to the sensitive crystals of membrane proteins (such as the entire PSII core complex), which are susceptible to mechanical shock and are strongly affected by small changes in humidity (Moraes *et al.*, 2014).

Crystals were thus deliberately cross-linked by placing the open end of the capillary over a reservoir of 25% glutaraldehyde in an adaptation of the method pioneered by Lusty (1999). The capillary was scored with a triangular diamond

Table 3
Data collection and processing.

Values in parentheses are for the outer shell.

Diffraction source	MaNDi, SNS
Wavelength (Å)	2–4
Temperature (K)	293
Detector	Anger camera
Crystal-to-detector distance (mm)	450
Rotation range between images (°)	10
Total rotation range (°)	80
Exposure time per image (h)	18
Space group	$P6_122$
a, b, c (Å)	55.92, 55.92, 194.95
α, β, γ (°)	90, 90, 120
Resolution range (Å)	13.97–2.30 (2.38–2.30)
No. of unique reflections	7326
Completeness (%)	84.21 (82.87)
Multiplicity	4.98 (3.09)
$\langle I/\sigma(I)\rangle$	8.36 (3.6)
$R_{\rm r.i.m.}$ (%)	22.8 (28.9)
$R_{\rm p.i.m.}$ (%)	8.10 (13.7)
Overall B factor from Wilson plot (Å^2)	21.8

needle file and snapped so that the crystal remained within a few millimetres of solvent at the open end. The capillary was then suspended in the upper half of an HPLC-vial insert over 20 µl fresh glutaraldehyde (Sigma–Aldrich, catalogue No. G5882). The gap was sealed with Parafilm and the setup was incubated for 1 h.

Surprisingly, this method also detached all of the crystals that were previously tightly attached to the capillary wall, but it is uncertain whether this observation was a result of cross-linking or of a change in humidity. Crystals were then flushed from the capillary by injecting a harvesting solution using a Hamilton syringe coupled by *via* short piece of silicone tubing to the other end of the capillary and washed in a deuterated harvesting solution (25% PEG 400, 50 m*M* $CaCl_2$, 100 m*M* MES–NaOH pH 6), transferred to a fresh 500 µl reservoir of the same buffer and incubated for several hours at 18°C. At the end of each of the described crystal-handling steps, test crystals were cryocooled straight from their buffer and tested by X-ray diffraction. Cross-linked crystals showed little difference in unit-cell size, mosaicity (determined with *labelit.index*; Sauter & Poon, 2010), resolution or spot shape compared with untreated crystals (see Supplementary Fig. S2). When challenged by transfer to water they did not dissolve, and when transferred to harvesting solution containing ethylene glycol in place of PEG 400 the X-ray diffraction at 100 K was not affected. However, the long-term stability at room temperature in a buffer significantly different from the crystallization solution appeared uncertain.

We therefore elected to cross-link crystals, wash them in the above D_2O-containing harvesting solution and mount them in a fresh capillary for shipping and data collection. These crystals were drawn back into 1 mm quartz glass capillaries and separated from precipitant solution to reduce the background during data collection. The capillaries were placed in 2 mm grooves cut into a perspex block, insulated from temperature changes and vibrations, and then shipped at ambient temperature to ORNL for data collection on the MaNDi instrument. A representative neutron diffraction image is shown in Fig. 2 and data-collection statistics for the initial data set are given in Table 3.

Refinement of the neutron data is currently under way using *phenix.refine* (Adams *et al.*, 2010). Of interest in the neutron diffraction structure will be the position and the orientation of surface water molecules, as earlier X-ray crystal structures showed the potential for water–carboxylate clusters that could facilitate fast Grotthus-type proton transfer along the protein surface.

Acknowledgements

The research at ORNL's Spallation Neutron Source was sponsored by the Scientific User Facilities Division, Office of Basic Energy Sciences, US Department of Energy. The Office of Biological and Environmental Research supported research at Oak Ridge National Laboratory's Center for Structural Molecular Biology (CSMB), using facilities supported by the Scientific User Facilities Division, Office of Basic Energy Sciences, US Department of Energy. For crystal screening, we acknowledge access to beamline P11 at PETRA III, DESY and beamlines 14.1 and 14.3 of the BESSY II storage ring (Berlin, Germany) *via* the Joint Berlin MX-Laboratory sponsored by the Helmholtz Zentrum Berlin für Materialien und Energie, the Freie Universität Berlin, the Humboldt-Universität zu Berlin, the Max-Delbrück-Centrum and the Leibniz-Institut für Molekulare Pharmakologie. We thank the members of the MX group at HZB and the P11 group at PETRA III for technical support. We would like to thank Rana Ali, Ruchira Chatterjee, Mohamed Ibrahim and Jan Kern for crystal handling and assistance during data collection and Rainer Dietrich for milling a Perspex capillary holder for room-temperature shipping.

Funding information

The authors thank the Deutsche Forschungsgemeinschaft (DFG) for financial support to the Collaborative Research Centre on 'Protonation Dynamics in Protein Function' (SFB1078, projects A5-Zouni/Dobbek and A4-Dau).

References

Adams, P. D. *et al.* (2010). *Acta Cryst.* D**66**, 213–221.
Ädelroth, P. & Brzezinski, P. (2004). *Biochim. Biophys. Acta*, **1655**, 102–115.
Afonine, P. V., Mustyakimov, M., Grosse-Kunstleve, R. W., Moriarty, N. W., Langan, P. & Adams, P. D. (2010). *Acta Cryst.* D**66**, 1153–1163.
Ago, H., Adachi, H., Umena, Y., Tashiro, T., Kawakami, K., Kamiya, N., Tian, L., Han, G., Kuang, T., Liu, Z., Wang, F., Zou, H., Enami, I., Miyano, M. & Shen, J.-R. (2016). *J. Biol. Chem.* **291**, 5676–5687.
Arnold, O. *et al.* (2014). *Nucl. Instrum. Methods Phys. Res. A*, **764**, 156–166.
Bergfors, T. (2003). *J. Struct. Biol.* **142**, 66–76.
Biertümpfel, C., Basquin, J., Suck, D. & Sauter, C. (2002). *Acta Cryst.* D**58**, 1657–1659.
Blakeley, M. P. (2009). *Crystallogr. Rev.* **15**, 157–218.
Bommer, M., Bondar, A. N., Zouni, A., Dobbek, H. & Dau, H. (2016). *Biochemistry*, **55**, 4626–4635.
Bondar, A.-N. & Dau, H. (2012). *Biochim. Biophys. Acta*, **1817**, 1177–1190.

Burkhardt, A., Pakendorf, T., Reime, B., Meyer, J., Fischer, P., Stube, N., Panneerselvam, S., Lorbeer, O., Stachnik, K., Warmer, M., Rodig, P., Gories, D. & Meents, A. (2016). *Eur. Phys. J. Plus*, **131**, 56.
Campbell, J. W., Hao, Q., Harding, M. M., Nguti, N. D. & Wilkinson, C. (1998). *J. Appl. Cryst.* **31**, 496–502.
Chayen, N. E. (2005). *Prog. Biophys. Mol. Biol.* **88**, 329–337.
Coates, L., Cuneo, M. J., Frost, M. J., He, J., Weiss, K. L., Tomanicek, S. J., McFeeters, H., Vandavasi, V. G., Langan, P. & Iverson, E. B. (2015). *J. Appl. Cryst.* **48**, 1302–1306.
Coates, L., Stoica, A. D., Hoffmann, C., Richards, J. & Cooper, R. (2010). *J. Appl. Cryst.* **43**, 570–577.
De Las Rivas, J. & Barber, J. (2004). *Photosynth. Res.* **81**, 329–343.
Del Val, C. & Bondar, A. N. (2017). *Biochim. Biophys. Acta*, **1858**, 432–441.
Ferreira, K. N., Iverson, T. M., Maghlaoui, K., Barber, J. & Iwata, S. (2004). *Science*, **303**, 1831–1838.
García-Ruiz, J. M., Novella, M. L., Moreno, R. & Gavira, J. A. (2001). *J. Cryst. Growth*, **232**, 165–172.
Gavira, J. A., Hernandez-Hernandez, M. A., Gonzalez-Ramirez, L. A., Briggs, R. A., Kolek, S. A. & Shaw Stewart, P. D. (2011). *Cryst. Growth Des.* **11**, 2122–2126.
Hellmich, J., Bommer, M., Burkhardt, A., Ibrahim, M., Kern, J., Meents, A., Müh, F., Dobbek, H. & Zouni, A. (2014). *Structure*, **22**, 1607–1615.
Ifuku, K. (2015). *Biosci. Biotechnol. Biochem.* **79**, 1223–1231.
Kita, A. & Morimoto, Y. (2016). *Mol. Biotechnol.* **58**, 130–136.
Koma, D., Sawai, T., Harayama, S. & Kino, K. (2006). *Appl. Microbiol. Biotechnol.* **73**, 172–180.
Lorch, S., Capponi, S., Pieront, F. & Bondar, A.-N. (2015). *J. Phys. Chem. B*, **119**, 12172–12181.
Lusty, C. J. (1999). *J. Appl. Cryst.* **32**, 106–112.
Moraes, I., Evans, G., Sanchez-Weatherby, J., Newstead, S. & Shaw Stewart, P. D. (2014). *Biochim. Biophys. Acta*, **1838**, 78–87.
Mueller, U., Förster, R., Hellmig, M., Huschmann, F. U., Kastner, A., Malecki, P., Pühringer, S., Röwer, M., Sparta, K., Steffien, M., Ühlein, M., Wilk, P. & Weiss, M. S. (2015). *Eur. Phys. J. Plus*, **130**, 141.
Nakamura, A., Ishida, T., Fushinobu, S., Kusaka, K., Tanaka, I., Inaka, K., Higuchi, Y., Masaki, M., Ohta, K., Kaneko, S., Niimura, N., Igarashi, K. & Samajima, M. (2013). *J. Synchrotron Rad.* **20**, 859–863.
Ng, J. D., Baird, J. K., Coates, L., Garcia-Ruiz, J. M., Hodge, T. A. & Huang, S. (2015). *Acta Cryst.* F**71**, 358–370.
Nikitina, J., Shutova, T., Melnik, B., Chernyshov, S., Marchenkov, V., Semisotnov, G., Klimov, V. & Samuelsson, G. (2008). *Photosynth. Res.* **98**, 391–403.
Nowaczyk, M., Berghaus, C., Stoll, R. & Rögner, M. (2004). *Phys. Chem. Chem. Phys.* **6**, 4878–4881.
O'Dell, W. B., Bodenheimer, A. M. & Meilleur, F. (2016). *Arch. Biochem. Biophys.* **602**, 48–60.
Oksanen, E., Chen, J. C.-H. & Fisher, S. Z. (2017). *Molecules*, **22**, 596.
Popelkova, H. & Yocum, C. F. (2011). *J. Photochem. Photobiol. B*, **104**, 179–190.
Roose, J. L., Frankel, L. K., Mummadisetti, M. P. & Bricker, T. M. (2016). *Planta*, **243**, 889–908.
Sauter, C., Balg, C., Moreno, A., Dhouib, K., Théobald-Dietrich, A., Chênevert, R., Giegé, R. & Lorber, B. (2009). *J. Appl. Cryst.* **42**, 279–283.
Sauter, C., Lorber, B., Kern, D., Cavarelli, J., Moras, D. & Giegé, R. (1999). *Acta Cryst.* D**55**, 149–156.
Sauter, N. K. & Poon, B. K. (2010). *J. Appl. Cryst.* **43**, 611–616.
Shaw Stewart, P. D., Kolek, S. A., Briggs, R. A., Chayen, N. E. & Baldock, P. F. M. (2011). *Cryst. Growth Des.* **11**, 3432–3441.
Shutova, T., Klimov, V. V., Andersson, B. & Samuelsson, G. (2007). *Biochim. Biophys. Acta*, **1767**, 434–440.
Sibanda, B. L., Blundell, T. L. & Thornton, J. M. (1989). *J. Mol. Biol.* **206**, 759–777.
Simpson, E. R., Meldrum, J. K., Bofill, R., Crespo, M. D., Holmes, E. & Searle, M. S. (2005). *Angew. Chem.* **44**, 4939–4944.
Tomanicek, S. J., Standaert, R. F., Weiss, K. L., Ostermann, A., Schrader, T. E., Ng, J. D. & Coates, L. (2013). *J. Biol. Chem.* **288**, 4715–4722.
Umena, Y., Kawakami, K., Shen, J.-R. & Kamiya, N. (2011). *Nature (London)*, **473**, 55–60.
Wan, Q., Parks, J. M., Hanson, B. L., Fisher, S. Z., Ostermann, A., Schrader, T. E., Graham, D. E., Coates, L., Langan, P. & Kovalevsky, A. (2015). *Proc. Natl Acad. Sci. USA*, **112**, 12384–12389.
Wei, X., Su, X., Cao, P., Liu, X., Chang, W., Li, M., Zhang, X. & Liu, Z. (2016). *Nature (London)*, **534**, 69–74.
Wheeler, M. J., Russi, S., Bowler, M. G. & Bowler, M. W. (2012). *Acta Cryst.* F**68**, 111–114.
Zouni, A., Witt, H. T., Kern, J., Fromme, P., Krauss, N., Saenger, W. & Orth, P. (2001). *Nature (London)*, **409**, 739–743.